Resolving complex structures at oncovirus integration loci with conjugate graph

Wenlong Jia[1,+], Chang Xu[1,+], and Shuai Cheng Li[1,*]

[1]Department of Computer Science, City University of Hong Kong, Kowloon Tong, Hong Kong

[+] These authors contributed equally to this work.

[*] To whom correspondence should be addressed.

Abstract

Oncovirus integrations cause copy number variations (CNVs) and complex structural variations (SVs) on host genomes. However, the understanding of how inserted viral DNA impacts the local genome remains limited. The linear structure of the oncovirus integrated local genomic map (LGM) will lay the foundations to understand how oncovirus integrations emerge and compromise the host genome' s functioning. We propose a conjugate graph model to reconstruct the rearranged local genomic map at integrated loci. Simulation tests prove the reliability and credibility of the algorithm. Applications of the algorithm to whole-genome sequencing data of Human papillomavirus (HPV) and hepatitis B virus (HBV)-infected cancer samples gained biological insights on oncovirus integrations. We observed five affection patterns of oncovirus integrations from the HPV and HBV-integrated cancer samples, including the exon loss, promoter gain, hyper-amplification of tumor gene, the viral cis-regulation inserted at the single intron and at the intergenic region. We found that the focal duplicates and host SVs are frequent in the HPV-integrated LGMs, while the focal deletions and complex virus SVs are prevalent in HBV-integrated LGMs. Furthermore, with the results yields from our method, we found the enhanced microhomology-mediated end joining (MMEJ) might lead to both HPV and HBV integrations, and conjectured that the HPV integrations might mainly occur during the DNA replication process. The conjugate graph algorithm code and LGM construction pipeline, available at https://github.com/deepomicslab/FuseSV.

Keywords:

virus integration, structural variation, complex structure, conjugate graph, cancer genomics

Key points:

- Conjugate graph model resolves complex local genomic strcuture at oncovirus integration loci.
- Local genome maps reveal five affection patterns of oncovirus integrations.
- Microhomology bases and small insertions are enriched at the junctions of structural variations and virus integrations.
- HPV and HBV integrations may be induced by the enhanced microhomology-meditated mechanism.

Introduction

Oncovirus integrations (VITs) could induce cancer genome instability [1-5], emerging as copy number variations (CNVs) and complex structural variations (SVs). Adjacent genes to the integrated sites are frequently dysregulated, such as TERT in hepatocellular carcinoma [5, 6] and MYC in cervical carcinoma [7, 8]. However, the explicit structure of the rearranged local genomic map (LGM) remains elusive. Some studies have reported the local maps at the integration site of human papillomavirus (HPV). Adey et al. resolved the haplotype of the HeLa cell line and HPV18-integrated genomic locus by consolidating results from a range of sequencing technologies, including the whole-genome shotgun sequencing, the fosmid mate-pair library with large insert size, and PacBio single-molecule sequencing data [1]. Akagi et al. constructed manually preliminary LGMs flanking integration sites in HPV-positive samples [2], including head and neck squamous cell carcinomas (HNSCC) and cervical cancers. However, oncovirus integrations demand the resolved local maps systematically, which would lead to more insights. Accurate LGMs analysis lays the foundations to understand how oncovirus integrations emerge and compromise the host genome's functioning. A computational model and algorithm are necessary to obtain the local genomic maps.

Although a growing number of studies examined the oncovirus integration effects on the expression regulations and genome stability in the flanking host genomic regions [6-13], our understanding of how inserted viral DNA influences the local genome remains limited. The LGMs can provide the haplotyping information to promote the investigation, such as the pairwise integrations, host and viral

rearrangements, inserted viral regulatory elements, and the copy number changes. Further, the LGM linear structure can facilitate the viral integration mechanism research with junction breakpoints phased together, as well as the alternative splicing and virus-host fusions. Several factors hinder the LGMs accurate construction, including the sequencing fluctuations, short genomic segments, repeated elements, and insufficient junction reads. Here, we introduce a graph-based algorithm to overcome these difficulties and construct LGMs at the oncovirus integration sites from cancer whole genome sequencing (WGS) data. Using multiple real and in silico datasets, we show that the algorithm is able to construct credible LGMs of oncovirus integrations and complex rearrangements on cancer genome. The LGM results further facilitate our investigation on the regulatory effects and formation mechanism accompanied by virus integrations.

Methods

Conjugate graph

We first consider the problem of reconstructing the disrupted genome with perfect NGS data and breakpoint detection, giving rise to no ambiguity. Based on the breakpoints, we derive two sets of reference genomic regions respectively from within (1) the human/host genome (denoted $H = \{h_1, h_2, \ldots, h_m\}$), and (2) the virus genome (denoted $V = \{v_1, v_2, \ldots, v_m\}$). Each region $s \in H \cup V$ can be either on the positive or the negative DNA chain, denoted s^+ and s^- respectively. Associated with each region s is a number $c(s)$ which indicates the copy number of the region.

We obtain from the NGS data a set J of junctions, each of which connects two regions in $H \cup V$. The junctions includes endogenous SVs on human and virus genome, VITs, and reference segment connections. Each $\mu \in J$ is an ordered pair $\langle u_i^{s_i}, u_j^{s_j} \rangle$, where $s_i, s_j \in \{+, -\}$ and $u_i, u_j \in H \cup V$. As DNA possesses a double helix structure, a junction segment is equivalent to its reverse complementary segment. Therefore, two junction segments $\langle u_i^{s_i}, u_j^{s_j} \rangle$ and $\langle u_j^{-s_j}, u_i^{-s_i} \rangle$ are equivalent, where $-s_i$ denotes the reverse complementary chain of s_i. Note that junction segments are directed, that is, $\langle u_i^{s_i}, u_j^{s_j} \rangle$ is different from $\langle u_j^{s_j}, u_i^{s_i} \rangle$. Meanwhile, each $\mu \in J$ may also occur multiple times in NGS data, denoted by $c(\mu)$, indicating the copy number of sequencing reads (i.e., split-reads) crossing a junction.

A directed graph $G = (U, E)$ is hence constructed from the NGS data, where the vertices $U = \{u^+, u^- \mid u \in H \cup V\}$ and edges $E = \mathrm{J}$. Given that H, V, J, and c contain no error, then

- G is connected.
- $\langle u_i^{s_i}, u_j^{s_j} \rangle \in E$ if and only if $\langle u_j^{-s_j}, u_i^{-s_i} \rangle \in E$, and
- a path that visits each vertex $u \in U$ exactly $c(u)$ times, and each edge exactly $c(\mu)$ times exists.

We refer to $\langle u_i^{s_i}, u_j^{s_j} \rangle$ and $\langle u_j^{-s_j}, u_i^{-s_i} \rangle$ as conjugate edges, and the vertices u^+ and u^- as conjugate vertices. We call the resultant graph a conjugate graph.

Local genomic map

Local genomic map (LGM) is defined as a path over the conjugate graph, where each $u \in H \cup V$ is visited exactly $c(u)$ times, and each $\mu \in \mathrm{J}$ is traversed exactly $c(\mu)$ times. Hence an LGM of length l gives us a sequence of visited vertices $(u_1^{s_1}, u_2^{s_2}, \ldots, u_l^{s_l})$ where $u_i \in H \cup V$ and $s_i \in \{+, -\}$. Without loss of generality, we assume that both the starting and ending point of an LGM are from the positive chain of the host, that is, $u_1^{s_1} = h_1^+$, $u_l^{s_l} = h_{\mathrm{m}}^+$. Note that we assume the path is along the positive strand. If the local genomic map contains a vertex of a negative strand, it implies an inversion event.

Existence of LGM in the conjugate graph

We show that it is possible to know if a conjugate graph G contains an LGM. Define the in-copy of a vertex u^s as the total copy number of edges with u^s as target vertex; that is, $in(u^s) = \sum c(\langle u_i^{s_i}, u^s \rangle)$. Similarly, we can define $out(u^s) = \sum c(\langle u^s, u_i^{s_i} \rangle)$.

Clearly, if G contains an LGM, then it satisfies the following properties:

(1) $c(u) = in(u^-) + out(u^+) = out(u^-) + in(u^+), \forall u \in H \cup V - \{h_1, h_{\mathrm{m}}\}$

(2) $c(h_1) = in(h_1^-) + out(h_1^+) = out(h_1^-) + in(h_1^+) + 1$, and

$c(h_{\mathrm{m}}) = in(h_{\mathrm{m}}^-) + out(h_{\mathrm{m}}^+) + 1 = out(h_{\mathrm{m}}^-) + in(h_{\mathrm{m}}^+)$

(3) A path exists from h_1^+ to u^+ or u^-, and a path exists from u^+ or u^- to h_{m}^+.

Note that, to form a path, we add a putative edge links sink vertex back to source vertex (property (2)). We refer to the properties (1) and (2) as degree balance, and property (3) as reachability.

An LGM of a conjugate graph shares similarities with an Eulerian path of an Eulerian Graph. The differences lie in that the vertices and edges are conjugated in LGMs. We adopt an algorithm derived from the Hierholzer's algorithm to find LGMs.

Similar to Hierholzer's algorithm, the algorithm for finding LGMs starts from an arbitrary vertex u_i^s, and recursively follow a trail of out-going edges from the vertex until returning to the vertex u_i^s itself, forming a circuit C. Due to the conjugation property, after we traverse an edge $\langle u_i^{s_i}, u_{i+1}^{s_{i+1}} \rangle$, the next edge with unused copy numbers we can choose from is either in the form of $\langle u_{i+1}^{s_{i+1}}, * \rangle$ or $\langle *, u_{i+1}^{-s_{i+1}} \rangle$, where $*$ represents a wildcard. Similar to the Eulerian path argument, as long as we have a vertex in the graph with unused copy numbers, the degree balance property ensures that it is always possible to find a circle that starts from and ends in the vertex. Therefore, given a vertex u_i^s in the circle C that still has unused copy numbers, we can find a new circle C' which can be merged with C to form a longer circular path. The above process is performed iteratively until we drain the copy numbers in the conjugate graph.

Theorem 1 A conjugate graph contains a local genomic map if and only if vertex u_i^+ or u_i^- of any region $u \in H \cup V$ is in a path from h_1^+ to h_m^+ or a path from h_m^- to h_1^-, and furthermore, u satisfies the degree balance condition.

Correcting the copy numbers

In the case of imperfect NGS data, the estimated copy numbers may contain fluctuations. The conjugate graph constructed would then lead to erroneous LGMs or no LGMs at all. To prevent such cases, we perform corrections to the graph under the principle that a corrected graph would contain an LGM, that is, the resultant conjugate graph should fulfill the two properties of reachability and degree balance.

It is possible to have missing edges or vertices due to reasons such as low sequencing depth and failure in detecting breakpoints which could break the property of reachability. To solve this in a parsimonious manner, we only consider the

insertion of additional edges that are likely to exist in a normal genome, such as $\langle h_1^+, h_2^+\rangle$, $\langle h_2^+, h_3^+\rangle$,..., $\langle h_{m-1}^+, h_m^+\rangle$, $\langle v_1^+, v_2^+\rangle$, $\langle v_2^+, v_3^+\rangle$,..., $\langle v_{n-1}^+, v_n^+\rangle$, and $\langle v_n^+, v_1^+\rangle$ if the virus in question has a circular DNA structure.

We propose an integer linear programming approach to address the degree balance property. Assign each region u and each junction μ to a target copy number $t(u)$ or $t(\mu)$ (Equations 1d and 1e), respectively, to satisfy the degree balance property (Equation 1b). The objective is to minimize the disagreement between the observed copy number and the target copy number (Equation 1a).

minimize

$$\sum_u \varepsilon_u + \sum_\mu \varepsilon_\mu \tag{1a}$$

subject to

$$in(u) = out(u) = t(u) \qquad \forall u \in H \cup V \tag{1b}$$

$$t(h_1) = t(h_m) \tag{1c}$$

$$-\varepsilon_u \leq c(u) - t(u) \leq \varepsilon_u \qquad \forall u \in H \cup V \tag{1d}$$

$$-\varepsilon_\mu \leq c(\mu) - t(\mu) \leq \varepsilon_\mu \qquad \forall \mu \in J \tag{1e}$$

$$\varepsilon_u, \varepsilon_\mu \in \mathbb{R}^+ \tag{1f}$$

$$t(u), t(\mu) \in \mathbb{Z}^+ \tag{1g}$$

Additional domain knowledge can be incorporated to further refine the linear programming process. For instance, the copy number of a virus DNA segment can be easily overestimated due to the existence of free virus in cells and other viral integration sites, and the copy number of DNA segments too short can be underestimated due to alignment difficulties. In those circumstances, we may assign lower penalty to the change of their copy numbers during the integer linear programming. The virus can have much more copy number than tumor genomes, due to the free virus genome and other viral integration sites. Considering this point, our model does not ask the copy numbers of virus genomic segments to be fully used in the LGMs. In our model, we assigned small weights to the viral segments, which allows excessive virus copies out of the current LGM if necessary.

Finding LGM

Our basic algorithm identifies an LGM path by iteratively selecting edges with non-zero weight at random to find circuits (called unit-cycles) and merge them. When determining the order of unit-cycles to be merged, the basic algorithm has no preference for any one possible LGM over the others. Principles of parsimony can be adopted; for instance, reference edges are preferred over edges that cross SVs or VITs breakpoints.

Simulation evaluation

One subtype (B2) of HBV and two subtypes (HPV16 and HPV18) of HPV are chosen to simulate virus integrations. Virus reference genome was randomly divided into segments. Integration sites in human reference genome (GRCh37) were randomly chosen inside reported integration hotspot regions (near gene TERT, CCNE1, KMT2B for HBV, LRP1B, FHIT for HPV16 and at the upstream of MYC for HPV18). Lengths of segments are random values within empirical ranges based on our research (2000-35000bp for each human segment, 1000-4000bp and 500-2000bp for each HPV and HBV segment respectively). Human and virus segments were then concatenated with regard to the different integration modes (**Supplementary Figure S1**) and saved as FASTA format files.

Simulated sequencing was performed using SAMtools (v1.3) wgsim utility at 30X average depth and 150bp read length [14]. Lower average depth (15X) is also introduced to complex integration cases to test algorithm's sensitivity. Since wgsim simulates all bases with the same quality score, we have also replaced the quality value of each sequence with qualities from actual 150bp sequencing data to resemble real sequencing results. Simulated sequencing reads are aligned back to human reference genome. Depth of each segment is calculated using SAMTools (v1.3, depth command) on uniquely mappable regions. Sequence mappability is determined by performing a 150bp read length simulated sequencing and aligning back to human genome. Regions covered by multiple-mapped reads are excluded in depth calculation.

All simulated samples are considered to have homogeneous integrations. Integration breakpoints are called by FuseSV. Structural variations on human and

virus genome are called by Meerkat [15] and seeksv [16]. Local genomic map of all simulated cases are recovered by the algorithm. Complex cases can have multiple possible LGMs.

Evaluation of integer linear programming

Test were performed to evaluate the robustness of the linear programming approach. We chose six simulated samples with large segment counts and tandem duplications, and then randomly assign fluctuations to segments' depth. The fluctuation values are within $[-c_{avg}/2, c_{avg}/2]$ where c_{avg} is the average haploid sequencing depth. The randomization is done 1000 times for each chosen samples and we performed linear programming for each iteration. 98% of all 6000 cases are corrected to our expected copy number profile. The other 2% cases had unit-cycles with one more or one less copy, still representing the correct LGM structure.

WGS data analysis

Tumor samples from cell lines have no corresponding normal sample. From our data repository, we selected a normal sample with no CNV at known integration regions. WGS data was aligned to human reference genome (GRCh37) using BWA [17]. HPV and HBV integrations are detected by FuseSV. Meerkat [15] and seeksv [16] are used to call structural variations on human and viral genome. CNV profile, tumor purity and ploidy are generated by Patchwork [18]. Segment depths were normalized against GC bias by deepTools [19].

Copy number calculation of segments and junctions in LGM

In tumor and control samples, the average depth of each host segment was calculated from GC-bias corrected alignments using SAMtools depth utility with minimum base and mapping quality set as 5 and 10, respectively. Call the purity of tumor-cell in tumor sample as $Purity_t$, the average ploidy of pure tumor-cell in tumor sample as $Ploidy_t$, both $Purity_t$ and $Ploidy_t$ are from Patchwork result [18]. And the average ploidy of pure normal cell as $Ploidy_n$(assumed as 2). The average ratio of the DNA from normal cells ($Ratio_n$) in each genomic region was calculated as below:

$$Ratio_n = 1 - \frac{Purity_t \times Ploidy_t}{Purity_t \times Ploidy_t + (1 - Purity_t) \times Ploidy_n} \qquad (2a)$$

For each host segment, the germline copy ratio of control normal sample ($CopyRatio_n$) can be obtained from WGS data (generally is one). The depth of this segment from pure tumor-cell in tumor sample ($Depth_t$) could be obtained from the observed segment average depth ($Depth_o$) and the whole genome average depth ($Depth_g$) via formula

$$Depth_t = Depth_o - Depth_g \times Ratio_n \times CopyRatio_n \qquad (3a)$$

To calculate the copy number of each host segment, the haploidy depth ($HaploDepth_t$) corresponding to single copy (CN=1) in the tumor cell could be obtained via formula

$$HaploDepth_t = \frac{Depth_g}{Purity_t \times Ploidy_t + (1 - Purity_t) \times Ploidy_n} \qquad (4a)$$

The copy number of each host segment is obtained from its depth ($Depth_t$) divided by the $HaploDepth_t$. Similarly, the copy numbers of VITs and SVs are calculated from the split-reads count divided by the $HaploDepth_t$. The copy numbers of viral segments are also obtained from the viral $Depth_t$ divided by the $HaploDepth_t$. Note that the $Depth_t$ of viral segment is calculated via formulas (2a) and (3a) with both $CopyRatio_n$ and $Ploidy_n$ set as zero, as we assumed all viral segments are reserved in tumor cells. The major and minor copy numbers (integer) of LGM region are determined from Patchwork CNV result [18], where we can get the objective copy number (integer) of the bilateral segments (source and sink) of LGM.

Construction of virus genome in each sample

We extract the unmapped and soft-clipped reads from alignment results of WGS and realign these reads to HPV and HBV references from the NCBI nucleotide database. The viral subtype with the most uniquely aligned reads and coverage of at least 20% was selected as the major one. Mutations (SNV and InDel) are detected in an iterative process to amend the viral genome sequence until no more mutations can be identified. This procedure is also adopted in our previous study [4]. The constructed viral genome is applied in the subsequent viral integration and LGM analyses of the corresponding cancer sample. Two reads types (span-reads and split-reads) are sought to support the viral integrations.

Microhomology at the junction sites

Microhomology bases (MHs) are detected at the junction sites of viral integrations and structural variations. Two types of MH bases are considered: the aligned and slipped MHs. Basically, the aligned microhomology is vertically matched bases covering or flanking the junction site, and the slipped microhomology has offset between the matched bases [20]. The slipped MH bases are required to have $\geq 3bp$ size and at least one base overlap. Criteria to determine the MH existence: i) the MH bases ($\geq 2bp$) must cover or locate next to the junction site, or ii) locate in flanking region ($\leq 5bp$) of the junction site and the MH size must be $\geq 4bp$ according our previous finding [7], or iii) merge 1bp-gaped neighbor MH bases and subject to the second criterion.

Results

Conjugate graph to construct local genomic map

Based on the breakpoints of VITs and SVs, both the host local genome and viral genome are divided into segments (**Figure 1A-B**), as vertices in the graph model (**Figure 1D**). Copy numbers (CNs) of segments are as the weights of vertices. Junctions of SVs and VITs are modeled as directed edges connecting two vertices, and their split-reads counts are converted to CN as the weights of the edges (**Figure 1C-D**). Integer linear programming is applied to correct weights of vertices and edges to reduce segment depth fluctuations, as well as compliment insufficient split-reads. As genome DNA has double strands, the vertices or edges are conjugated, i.e, a vertex or an edge and their reverse complementary counterparts and share the respective weights. We then use an algorithm modified from the Eulerian Circuits traversal rule to find available circular paths (called unit-cycles, **Figure 1E**), and then merge them to construct the local genomic map consisting of host and virus segments (**Figure 1F**).

In our algorithm, the first upstream and last downstream host segments are called the source and sink vertices of the conjugate graph (**Figure 1D-E**) respectively. The algorithm first finds the main path, which starts from the source vertex and extends along the edges with non-zero weight until it reaches the sink vertex (**Figure 1E**). If a vertex or an edge is included in the path, its weight on the graph decreases by one.

Then, starting at a vertex with non-zero weight left, our algorithm forms a unit-cycle by randomly walking along edges with non-zero weight until the vertex itself has reached again. More unit-cycles can be found iteratively until the all the weights are drained. Finally, all unit-cycles are merged with the main path to get putative LGMs. Due to the random walking and merging of the unit-cycles, there could be multiple LGM candidates generated from the conjugate graph, and our algorithm will report all possible LGMs.

Evaluation on in silico data

To evaluate the reliability of the conjugate graph algorithm, we simulated a set of oncovirus integration LGMs at genomic loci of well-known hotspot genes, including HBV integrations (TERT, CCNE1, and KMT2B) [11] and HPV integrations (LRP1B, FHIT, and MYC) [7]. Combining the different SV types, copy numbers, and viral segments, we generated eight LGM simulated modes in each gene locus, such as substitutive integrations, inversed insertions, and complex tandem duplications (**Supplementary Figure S1**). In total, we prepared simulated sequencing data of 48 LGM cases for evaluation (**Supplementary Table S1**). The conjugate graph algorithm successfully recovered all simulated LGMs at HBV and HPV integrated sites. The integer linear programming obtained the copy numbers of all segments and junctions (SVs and VITs) with zero offset from the expected values. Moreover, for complex structures with high CN segments, the algorithm reported other possible candidate genomic maps that also satisfy the observed conjugate graph. The performance on in silico data supports the reliability of the conjugate graph to resolve diverse local genomic maps.

On WGS data of HPV-integrated cervical cancers

We first applied the developed method to reconstruct the LGMs at HPV integration loci in four cervical carcinoma samples (T4931, T6050, HeLa, and SiHa) [7]. All samples have arm-level copy number changes of the HPV-integrated chromosomes (**Supplementary Figure S2**). The conjugate graph algorithm constructed LGMs of all validated HPV integrations with most CN offsets less than one (73.3%, **Supplementary Table S2** and **S3**).

First, the LGM on unbalanced polyploidy was successfully constructed in sample T4931. The HPV16 integrations locate at gene GLI2 locus on chr2q (heterozygous

pentaploid, minor CN = 2, **Supplementary Figure S2A**). As the integration might locate on the paternal or maternal chromosomes, our method algorithm provides two LGM candidates (**Figure 2** and **Supplementary Figure S3**). The resolved LGM consists of two unit-cycles containing three virus integrations (VITs), virus circularization (V-CIRC), one viral inversion, and one host tandem duplication (**Figure 2C**). The HPV segments carry complete viral long control region (LCR) and insert at the intron region of gene GLI2.

Second, we solved the LGM with asymmetric copy of the source and sink vertices. The chr8q of HeLa cell line shows different copy numbers at the HPV18 integrated sites: the upstream and downstream are tetraploid and hexaploid respectively, both of which are heterozygous (minor CN = 1, **Supplementary Figure S2B**). Previous study has reported that the HPV18 integrates on the major allele of the tetraploid [1]. The constructed LGM contains three unit-cycles consisting of four VITs and the V-CIRC (**Supplementary Figure S4**). The unit-cycles are evenly distributed in the three copies of the major allele. The LGM structure is similar to the reported [1], but with different copy numbers and breakpoints of the unit-cycles.

Third, two LGMs appeared as diploid with loss of heterozygosity (LOH). Both of the T6050 sample and SiHa cell line have HPV16 integrations at chr13q (LOH, **Supplementary Figure S2C-D**). The LGM of T6050 contains one unit-cycle consisting of two VITs, the V-CIRC, and one host tandem duplication at the gene KLF12 locus (**Supplementary Figure S5**). Interestingly, this unit-cycle has different copy times (two and three) in the remained diploid alleles, implying the possible existence of circular extrachromosomal DNA (ecDNA). The SiHa cell line has two unit-cycles in the LGM at the HPV16 integration sites (downstream of the gene KLF12, **Supplementary Figure S6**). The unit-cycles contain two VITs, the V-CIRC, one viral deletion, and one host deletion. The structure of the unit-cycles is the same as in the previous reports [2].

On WGS data of HPV-integrated HNSCC cancers

We then applied the conjugate graph algorithm on two HPV16-positive HNSCC cell lines (UM-SCC-47 and UPCI-SCC090) [2]. The resolved HPV16-integrated LGMs are more complex than the four cervical cancers. Different from the published preliminary results [2], our method reported all detected genomic segments and breakpoints.

The first LGM contains tandem duplication of partial gene body of tumor suppressor, and might lead to the truncation of the coding-frame. The UM-SCC-47 cell line has HPV16 integrations at the tumor suppressor TP63 locus on chr3q [21, 22]. The broad region (3q26.31-q29) shows heterozygous triploid (minor CN = 1), and the focal region (in q28) at the HPV16 integrations has prominent high copy number gains (**Supplementary Figure S7A**). In total, six HPV16 integrations and four endogenous rearrangements are considered to construct two LGMs (**Supplementary Table S4**) corresponding to the minor (**Supplementary Figure S8**) and major alleles (**Supplementary Figure S9**). Our algorithm successfully obtained five unit-cycles. Interestingly, all segments of the NO.1 unit-cycle are from the host genome and form a tandem duplication structural variation with an inner deletion (the 'H3' segment). The NO.3 and NO.4 unit-cycles both have high copy numbers (5 and 49 respectively) and mainly contribute to the focal gain on the host genome. The minor allele and major allele LGMs share the same unit-cycles and differ only in copy numbers.

Another LGM has focal hyper-amplification inducing the copy number gain of oncogene. The UPCI-SCC090 cell line has HPV16 integrations in chr6p21.2. The chr6 is heterozygous triploid (minor CN = 1), and the HPV-integrated focal region shows a higher copy number (**Supplementary Figure S7B**). The focal host region contains seven HPV16 integrations and six endogenous rearrangements. These breakpoints divide the host and virus genome into a total of 28 segments (**Supplementary Table S4**), significantly more than the other samples mentioned above. Two LGMs are constructed for virus integrations on the minor (**Supplementary Figure S10**) and major allele (**Supplementary Figure S11**), respectively. The minor allele LGM is formed by seven unit-cycles. The NO.1 unit-cycle crosses the host and viral genomes five times with inversions and integrations. The NO.6 and NO.7 unit-cycles mainly contribute to the high copy number of this focal region with 19 and 14 copies, respectively. The major allele LGM has a similar global structure but one more unit-cycle. This LGM involves multiple genes, such as PI16, FGD2, PIM1, and SNORD112. The proto-oncogene PIM1 is completely located in the 'H9' segment with a high copy number (CN = 58). In addition, after the LGM construction, the remaining HPV16 genome copies formed two types of free viral genome by our conjugate graph algorithm: the complete (CN = 655) and with deletion (CN = 22). Moreover, the remaining host segments might exist as the ecDNAs.

On WGS data of HBV-integrated hepatocellular carcinomas

Next, we applied the conjugate graph algorithm on the HBV-infected hepatocellular carcinomas (HCC). Six HCC samples were selected from the previous study that reported the genome-wide detection of HBV integrations [11]. Four samples have arm-level copy number changes of the HBV-integrated chromosomes, but none shows the focal gain at the integration sites (**Supplementary Figure S12**). The constructed LGMs further reveal that most of the inserted HBV DNA segments replace the host segments and consequently lead to the deletions on the human genome (**Supplementary Table S5** and **S6**, **Figure 3**, **Supplementary Figure S13-S17**), different from the tandem duplications induced by the HPV integrations. Additionally, the remaining HBV segment copies imply the free viral genomes in five samples.

There are two HBV-integrated LGMs located on the heterozygous diploid (62T and 182T, **Supplementary Figure S12A-B**). The sample 62T has three HBV integrations at the *MLL4* oncogene on chr19q13.12 (**Figure 3**). The LGM contains two unit-cycles. The NO.1 unit-cycle duplicates the 'H2' host segment covering the whole gene body of ZBTB32, the promoter and first two exons of *MLL4*, which are abundant of the regulatory element marks [23]. The structure is predicted to have no truncation effect on gene *MLL4* as the coding frame is completely preserved ('H2' to HBV to 'H3'). Furthermore, the inserted HBV segments ('V2' to 'V5') carry the enhancer II and core promoter [24, 25], which potentially promote the *MLL4* expression [11]. The HBV DNA segments inserted at gene NBAS on chr2p24.3 of sample 182T, and resulted in the deletion of the host segment ('H2') containing 14 exons of NBAS (**Supplementary Figure S13**). The resolved LGM has a simple structure that the 'H2' host segment is replaced by the majority of the HBV genome.

We found that the sample 13T and 260T both have copy number gains of broad regions at the HBV integration loci. The 13T has HBV integrations at the TERT gene locus on chr5p15.33, which is heterozygous triploid extending to p15.2 (**Supplementary Figure S12C**). As the second host segment ('H2', CN = 2, intron region) has one copy loss, we determined that the HBV integrated on the minor allele and replaced the 'H2' segment (**Supplementary Figure S14**). The HBV genome is divided into 16 segments by breakpoints of two integrations and seven viral rearrangements, which are all considered in the LGM construction. The inserted HBV DNA segments formed a complex structure consisting of four unit-cycles. The

unit-cycle NO.2 and NO.3 carry the HBV enhancers and core promoters, which might explain the elevated gene expression of TERT in this sample [11]. In sample 260T, the HBV integrated at the ANK3 gene on chr10 (heterozygous tetraploid, minor CN = 2, **Supplementary Figure S12D**). The resolved LGM contains two unit-cycles including two HBV integrations and three HBV SVs (**Supplementary Figure S15**). These two unit-cycles are completely composed of inserted HBV DNA segments and substitute the 'H2' host segment in two allele copies. Notably, our algorithm reports the unit-cycle NO.1 only in one allele, and it might exist in the form of ecDNA.

The remaining two HCC samples displayed arm-level LOH of HBV-integrated chromosomes (101T and 261T). The sample 101T has two HBV integrations at the GLRA2 gene locus in the chrXp22.2 (CN = 1). The remained heterozygous status of the chrXq supports the chrXp is an LOH (**Supplementary Figure S12E**). The LGM is simple and the only unit-cycle is the inserted 'V2' HBV segment that replaces the 'H2' host segment (partial intron of GLRA2, **Supplementary Figure S16**). In sample 261T, there are two HBV integrations located in the intron of BBS2 gene on chr16 (CN = 1, **Supplementary Figure S12F**). Similar to the sample 13T, the HBV genome is divided into 17 segments by two integrations and seven HBV SVs. Our algorithm reports the LGM consisting of three unit-cycles with all segments from the viral genome (**Supplementary Figure S17**). These unit-cycles have complex structures composed of deletion, tandem duplication, and inversions. Again, one host deletion ('H2') is caused by the inserted HBV DNA.

Diverse affection patterns of oncovirus integrations

According to the resolved LGMs, we summarized five affection patterns of the oncovirus integrations in our samples. Firstly, the integrations locate in a single intron, including the HPV16 in T4931 (gene GLI2), and the HBV in 13T (TERT), 101T (GLRA2), 260T (ANK3), and 261T (BBC2). The inserted viral DNA segments carry the epigenomic regulator elements, such as the long control region (LCR) of HPV, and the enhancers and core promoter of HBV, which might contribute to the local expression dysregulations. The abnormal alternative splicings are also reported in researches of both HPV and HBV integrations [2, 13]. Secondly, the LGM covers multiple exons in sample UM-SCC-47 (HPV16 at TP63) and 182T (HBV at NBAS), both likely lead to the truncation of the coding-frame. Thirdly, in sample UPCI-SCC090, the LGM contains focal hyper-amplifications harboring the complete

genes (PIM1 and SNORD112), which commonly relate to elevated expression and might induce tumorigenesis [26]. Fourthly, in sample 62T, tandem duplication doubles the promoter and maintains the complete coding-frame of MLL4, which is also possible subject to the inserted HBV enhancer and core promoter. Fifthly, both of T6050 sample and SiHa cell line have HPV integrations at the intergenic regions between gene KLF5 and KLF12, whose expressions are probably affected by the amplified HPV LCR in the LGM. The HeLa cell line has been reported that the inserted HPV segments have long-range chromatin interactions with downstream MYC gene, which has high RNA expression phased in the HPV-integrated haplotype [1]. This implicates the cis-regulation of HPV integration is possibly mediated by the epithelium specific viral enhancer remained in the LGMs.

Enhanced Microhomology-mediated mechanism of HPV and HBV integration

The resolved LGMs enable us to analyze the details of breakpoints and investigate the oncovirus integration mechanisms. Here, we propose that the slipped microhomology and the small junctional insertion (see **Methods**), which are the defining characteristic of the microhomology-mediated end joining [27, 28]. A previous study on cervical cancer has reported the enrichment of aligned microhomology at HPV integration sites [7]. In total, 54.05% (20/37) of virus integrations have aligned microhomology at the junction site. Meanwhile, the percentage became to 83.78% (31/37) when the slipped microhomology and the junctional insertion are considered (**Figure 4**, **Supplementary Table S8**, **Supplementary Figure S19-S26**), and it is more prevalent in HPV integrations (91.67%, 22/24) comparing with HBV (69.23%, 9/13). Moreover, microhomology and insertions are found at the junction sites of the majority (84.84%, 28/33) of the endogenous SVs: 100% (9/9) for host SVs in HPV LGMs, 83.33% (5/6) for HPV SVs, and 77.78% (14/18) for HBV SVs. Furthermore, the complex SVs in sample GBM0152 also shows similar phenomenon that 60% (12/20) of the SV junctions carry the microhomology (**Supplementary Table S7** and **S8**, **Supplementary Figure S18**, **S27** and **S28**). Microhomology enrichment supports the suggested replication-based mechanism, which generates these complex rearrangements in this sample [15].

We further propose that the enhanced microhomology-mediated end joining (MMEJ) may be the underlying mechanism of both HPV and HBV integrations together with the endogenous host and viral rearrangements in the local region. Each unit-cycle in the resolved LGMs has at least one boundary harboring the microhomology or junctional insertion (**Figure 5** for HPV16, **Supplementary Figure S29** for HPV18, and **Figure 6** for HBV), suggesting that the formation of each unit-cycle is possibly initialized via the replication-based template-switching event. The well-known alternative mechanisms of MMEJ include the fork stalling and template switching (FoSTeS) [29] and the microhomology-mediated break-induced replication (MMBIR) [30].

We hypothesize that the HPV integrations might mainly occur during the DNA replication process. All of the HPV-integrated LGMs harbor the focal duplications of human genomic segments (**Figure 5** and **Supplementary Figure S29**), while most (83%, 5/6) of the HBV-integrated LGMs only contain focal deletions caused by the substitution of the inserted viral segments (**Figure 6**). Additionally, most (83%, 5/6) of the HPV-integrated LGMs have host SVs, but none of the HBV-integrated LGMs has. These differences further enlightens us to hypothesize that the HPV integrations might mainly occur during the DNA replication process (i.e., the S phase during the mitosis) and form complex structure via the rolling circle replication [2, 31], and the HBV integrations likely arise under the DNA repairing circumstance and are prone to produce simple structure.

Discussion

The detection of the oncovirus integrations and structural variations is widely developed, and the effects and formation mechanisms of integrations are extensively studied. However, the investigation in the local genomic region with the linear complex structure remains limited. Our conjugate graph algorithm constructs the local genomic maps of HPV and HBV integrations. It provides details to research the regulatory influences on local genes and the underlying formation mechanisms, combining with the copy changes of rearranged host and viral genomic segments.

The local genomic map sometimes contains segments shorter than the insert-size of the paired-end sequencing data or harboring repeated DNA sequence, leading to the underestimated copy number calculation from the average depth of the relevant

segment. Similarly, the insufficient split-reads count also reduces the copy number of the SV and VIT junctions. These inaccurate copy numbers will hinder the accuracy of the LGM results. The integer linear programming in our algorithm overcomes such difficulties by assigning smaller weights for relevant vertex and edge in the graph model, and successfully construct the optimal LGM with minimum offsets.

The unit-cycles in the conjugate graph model are the basic structural units representing the connections of segments and junctions. Unit-cycles are merged in ways to form different LGM solutions. Due to the short reads in NGS data, the factual orders of merging cannot be determined technically. Here, we select the solution with the simplest structure to report, following Ocham's razor . The candidate LGMs could be further filtered based on the phased structure obtained from the advanced DNA sequencing, such as 10x long-range linked-reads and single-molecule reads. Furthermore, when the virus-integrated chromosome is heterozygous unbalanced polyploidy, it is difficult to determine whether the paternal or maternal allele carries the viral insertions based on short reads. The mutations phasing between the local genomic segments and the flanking regions of the constructed LGMs will help solve the problem. Multiple sequencing technology can provide this additional information, including the mate-pair library with large insert-size [1], 10x linked-reads [32], and Hi-C [33].

When the virus-integrated allele has more than one copy, our algorithm will try to distribute all relevant unit-cycles evenly among the multiple copies to minimize the differences. However, the actual count of the unit-cycles might change within different allele copies (e.g., **Supplementary Figure S5D** and **S6D**). According to the circular structure and common hyperamplification, the unit-cycles can be the circular extrachromosomal DNA, which needs more investigations in the future study, for example, the inter-chromosomal interactions from Hi-C data [34]. Recent studies have proved that the ecDNA promotes oncogene expressions and drives tumor evolution [35, 36]. The speculated oncovirus integrations related ecDNAs probably have similar carcinogenic functions.

From the constructed LGMs, we can get the structural investigation on the formation mechanism of the oncovirus integrations and endogenous SVs in the local genomic region. To our knowledge, this is the first time to combine the aligned/slipped microhomology and junctional insertion together in the mechanism research of viral integrations. The enrichment of microhomology and insertion

indicates that both the HPV and HBV integrations may be generated via the microhomology-mediated end joining (MMEJ), promoted during the HPV16 infection [37]. Furthermore, the focal duplicates and host SVs are frequent in the HPV-integrated LGMs, while the HBV-integrated LGMs are abundant in focal deletions and complex virus SVs. This apparent difference suggests that the formation circumstances of HPV and HBV integration may be different. To answer this question, it needs more samples and experiments in a future study.

In summary, we present a conjugate graph algorithm to construct the local genomic map of virus integrations mediated host and viral rearrangements from the whole genome sequencing data. The algorithm can normalize imperfect sequencing depths and elucidate the linear DNA structure at virus integration sites. The simulation tests and the applications on WGS data of cancer samples prove the reliability and credibility of our model. The results shed light on the genomic dysregulation and formation mechanism of the oncovirus integrations.

Data availability

The conjugate graph algorithm code, LGM analysis data of all samples (Supplementary Dataset zip file), and LGM construction pipeline demo are available in github repository (https://github.com/deepomicslab/FuseSV). The cancer whole genome sequencing data is obtained under SRA accession number SRA180295 [7], and EGA accession number EGAS00001000599 [2] and ERP001196 [11].

Author contributions

S.L. proposed the conjugate graph model and designed algorithm to obtain the LGM paths. W.J. and C.X. implemented and optimized the algorithms. W.J. and C.X. performed the WGS data analysis. C.X. performed the simulation work. W.J. developed the FuseSV. W.J. summarised and compared the viral integration features and mechanisms. W.J., C.X. and S.L. wrote and revised the manuscript. All authors reviewed the article and approved the final manuscript.

Author description

Wenlong Jia received his Ph.D. degree from the Department of Computer Science of City University of Hong Kong in 2019. His research interests include cancer genetics, bioinformatics, and computational biology.

Chang Xu received his master degree of computational data science from Carnegie Mellon University in 2019. His research interests include bioinformatics, algorithm development, and data mining.

Shuai Cheng Li is currently a professor and head of a lab at the Department of Computer Science of City University of Hong Kong. The Li lab develops various computational tools to gain insight into the interactions between omics data and disease phenotypes. Her research interests include genetics, bioinformatics, and machine learning.

Funding

This work was supported by the General Research Fund (GRF) Projects 9042348 (CityU 11257316).

Conflict of interest

Conflict of interest statement. None declared.

References

1. Adey A, Burton JN, Kitzman JO, et al. The haplotype-resolved genome and epigenome of the aneuploid HeLa cancer cell line. Nature 2013; 500:207 – 211.

2. Akagi K, Li J, Broutian TR, et al. Genome-wide analysis of HPV integration in human cancers reveals recurrent, focal genomic instability. Genome Res. 2014; 24:185 – 199.

3. Satou Y, Miyazato P, Ishihara K, et al. The retrovirus HTLV-1 inserts an ectopic CTCF-binding site into the human genome. Proc. Natl. Acad. Sci. U. S. A. 2016; 113:3054 – 3059.

4. Chen X-P, Long X, Jia W-L, et al. Correction to: Viral integration drives multifocal HCC during the occult HBV infection. J. Exp. Clin. Cancer Res. 2019; 38:480.

5. Kan Z, Zheng H, Liu X, et al. Whole-genome sequencing identifies recurrent mutations in hepatocellular carcinoma. Genome Res. 2013; 23:1422 – 1433.

6. Zhao L-H, Liu X, Yan H-X, et al. Genomic and oncogenic preference of HBV integration in hepatocellular carcinoma. Nat. Commun. 2016; 7:12992.

7. Hu Z, Zhu D, Wang W, et al. Genome-wide profiling of HPV integration in cervical cancer identifies clustered genomic hot spots and a potential microhomology-mediated integration mechanism. Nature Genetics 2015; 47:158 – 163.

8. Cancer Genome Atlas Research Network, Albert Einstein College of Medicine, Analytical Biological Services, et al. Integrated genomic and molecular characterization of cervical cancer. Nature 2017; 543:378 – 384.

9. Murakami Y, Saigo K, Takashima H, et al. Large scaled analysis of hepatitis B virus (HBV) DNA integration in HBV related hepatocellular carcinomas. Gut 2005; 54:1162 – 1168.

10. Zhao X, Liu Q, Cai Q, et al. Dr.VIS: a database of human disease-related viral integration sites. Nucleic Acids Research 2012; 40:D1041 – D1046.

11. Sung W-K, Zheng H, Li S, et al. Genome-wide survey of recurrent HBV integration in hepatocellular carcinoma. Nat. Genet. 2012; 44:765 – 769.

12. Ojesina AI, Lichtenstein L, Freeman SS, et al. Landscape of genomic alterations in cervical carcinomas. Nature 2014; 506:371 – 375.

13. Nault J-C, Datta S, Imbeaud S, et al. Recurrent AAV2-related insertional mutagenesis in human hepatocellular carcinomas. Nat. Genet. 2015; 47:1187 – 1193.

14. Li H, Handsaker B, Wysoker A, et al. The Sequence Alignment/Map format and SAMtools. Bioinformatics 2009; 25:2078 – 2079.

15. Yang L, Luquette LJ, Gehlenborg N, et al. Diverse mechanisms of somatic structural variations in human cancer genomes. Cell 2013; 153:919 – 929.

16. Liang Y, Qiu K, Liao B, et al. Seeksv: an accurate tool for somatic structural variation and virus integration detection. Bioinformatics 2017; 33:184 – 191.

17. Li H, Durbin R. Fast and accurate short read alignment with Burrows-Wheeler transform. Bioinformatics 2009; 25:1754 – 1760.

18. Mayrhofer M, DiLorenzo S, Isaksson A. Patchwork: allele-specific copy number analysis of whole-genome sequenced tumor tissue. Genome Biol. 2013; 14:R24.

19. Benjamini Y, Speed TP. Summarizing and correcting the GC content bias in high-throughput sequencing. Nucleic Acids Res. 2012; 40:e72.

20. Ottaviani D, LeCain M, Sheer D. The role of microhomology in genomic structural variation. Trends Genet. 2014; 30:85 – 94.

21. Flores ER, Sengupta S, Miller JB, et al. Tumor predisposition in mice mutant for p63 and p73: evidence for broader tumor suppressor functions for the p53 family. Cancer Cell 2005; 7:363 – 373.

22. Melino G. p63 is a suppressor of tumorigenesis and metastasis interacting with mutant p53. Cell Death Differ. 2011; 18:1487 – 1499.

23. ENCODE Project Consortium. An integrated encyclopedia of DNA elements in the human genome. Nature 2012; 489:57 – 74.

24. Kramvis A, Kew MC. The core promoter of hepatitis B virus. Journal of Viral Hepatitis 1999; 6:415－427.

25. Seeger C, Mason WS. Hepatitis B virus biology. Microbiol. Mol. Biol. Rev. 2000; 64.

26. Narlik-Grassow M, Blanco-Aparicio C, Carnero A. The PIM Family of Serine/Threonine Kinases in Cancer. Medicinal Research Reviews 2014; 34:136－159.

27. Bennardo N, Cheng A, Huang N, et al. Alternative-NHEJ is a mechanistically distinct pathway of mammalian chromosome break repair. PLoS Genet. 2008; 4:e1000110.

28. 28. McVey M, Lee SE. MMEJ repair of double-strand breaks (director’s cut): deleted sequences and alternative endings. Trends in Genetics 2008; 24:529－538

29. Lee JA, Carvalho CMB, Lupski JR. A DNA replication mechanism for generating nonrecurrent rearrangements associated with genomic disorders. Cell 2007; 131:1235－1247.

30. Hastings PJ, Ira G, Lupski JR. A microhomology-mediated break-induced replication model for the origin of human copy number variation. PLoS Genet. 2009; 5:e1000327.

31. Kusumoto-Matsuo R, Kanda T, Kukimoto I. Rolling circle replication of human papillomavirus type 16 DNA in epithelial cell extracts. Genes Cells 2011; 16:23－33.

32. Zheng GXY, Lau BT, Schnall-Levin M, et al. Haplotyping germline and cancer genomes with high-throughput linked-read sequencing. Nat. Biotechnol. 2016; 34:303－311.

33. Selvaraj S, R Dixon J, Bansal V, et al. Whole-genome haplotype reconstruction using proximity-ligation and shotgun sequencing. Nat. Biotechnol. 2013; 31:1111－1118.

34. Harewood L, Kishore K, Eldridge MD, et al. Hi-C as a tool for precise detection and characterisation of chromosomal rearrangements and copy number variation in human tumours. Genome Biol. 2017; 18:125.

35. Turner KM, Deshpande V, Beyter D, et al. Extrachromosomal oncogene amplification drives tumour evolution and genetic heterogeneity. Nature 2017; 543:122 – 125.

36. Wu S, Turner KM, Nguyen N, et al. Circular ecDNA promotes accessible chromatin and high oncogene expression. Nature 2019; 575:699 – 703.

37. Leeman JE, Li Y, Bell A, et al. Human papillomavirus 16 promotes microhomology-mediated end-joining. Proc. Natl. Acad. Sci. U. S. A. 2019; 116:21573 – 21579.

Figure Legends

Figure 1. Demo representation of Conjugate graph resolved LGM of HPV16 integrations. Breakpoints of SVs ('r') and VITs ('i') are represented by dashed and solid red lines respectively, by which the host local (**A**) and HPV16 (**B**) genomes are divided into segments (host: H1~H6; HPV: V1~V6) denoted with copy number (CN, yellow filled frame) adjusted by integer linear programming (ILP). (**C**) Variant segment junctions utilized in Conjugate graph, including VITs ('i'), SVs ('r') and viral circularization ('c') . Junctions are denoted as pairwise segment ID and strand with copy number adjusted by ILP. Note that segments in red frame are reverse complementary counterpart. (**D**) The Conjugate graph model with directed vertices and edges representing segments and junctions respectively. The conjugate property of vertex (positive and negative) and junction (bi-direction) corresponds to the double strands of DNA. Dots on vertices and circled numbers on edges denote the copy number adjusted by ILP. Dashed edges indicate the segment junctions along the reference genome. (**E**) The unit-cycle paths resolved from the Conjugate graph. The main path extends from the source vertex along non-zero weighted edges to the sink vertex. (**F**) The LGM after merging unit-cycles with the main path.

Figure 2. Presentative LGM at HPV integration sites (gene GLI2) on chr2 (minor allele) of the T4931 sample [7]. (**A**) Human genomic region flanking HPV integrations are divided into six segments (H1~H6, in different resolutions) by VITs (red solid-line) and SVs (red dashed-line) denoted with breakpoints. Depth spectrum is displayed with original (grey frame) and ILP-adjusted (yellow frame) copy numbers of segments. (**B**) Segmentation (V1~V6) of HPV16 genome by VITs and SVs. The segment (V3) less than 100bp is marked with red dot. (**C**) Variant segment junctions utilized in Conjugate graph. (**D**) Resolved alleles of the 'Simplest LGM' are indicated as string of coloured segments with copy times, including reference allele (major allele) and that harbours HPV16 integrations (minor allele). Sum of absolute offset of segments and junctions are shown. Unit-cycles (shadowed areas) in LGM are denoted with repeat time. Note that the unit-cycles might exist as circular extrachromosomal DNA (ecDNA).

Figure 3. Presentative LGM at HBV integration sites (gene MLL4) on chr19 (minor allele) of the 62T HCC sample [11]. (**A**) Human genomic region flanking HBV integrations are divided into three segments (H1 ~ H3) by VITs denoted with breakpoints. Depth spectrum is displayed with original (grey frame) and ILP-adjusted (yellow frame) copy numbers of segments. (**B**) Segmentation (V1 ~ V6) of HBV genome by VITs and SVs. The segment less than 100bp is marked with red dot. (**C**) Variant segment junctions utilized in Conjugate graph. (**D**) Resolved alleles of the 'Simplest LGM' are indicated as string of coloured segments with copy times, including reference allele and that harbours HBV integrations. Sum of absolute offset of segments and junctions are shown. Unit-cycles (shadowed areas) in LGM are denoted with repeat time. Note that the free HBV genomes might exist.

Figure 4. Alignment of the sequence around the integration site between the host and virus genome, and the endogenous rearrangements. In the samples (**A**) HeLa, (**B**) SiHa, (**C**) 62T, (**D**) 101T. The junction boundaries are shown as vertical dashed lines. All viral sequences are from the reference strand. Green, upstream junction partner; yellow, downstream junction partner; red, nucleotides that vertically align to both reference sequences (aligned microhomologous bases); pairwise numbered sticks, slipped microhomologous bases. All microhomologous bases follow the 5'-to-3' direction. The junction segment IDs are corresponding to the segments in the resolved LGMs.

Figure 5. Features of HPV16 integrated LGMs in five samples. Human genomic segments related to HPV16 integrated LGMs are shown as sectors with their relevant LGM path in sample specific colours. Segments of LGMs are denoted by numbered concentric arcs. The numbers, starting from 1, indicate the order in which each arc is visited starting from the source segment of an LGM. Each special symbol shown in "Path Abbreviated" section in the figure legends denotes an arc that is visited more than once in the LGM, such as the '+' symbol for NO.4 and NO.8 arcs in LGM of SiHa sample. Sequential segments in LGM could be merged in single arc (**Supplementary Table S9**). Repeat times of unit-cycles in LGMs are stated in figure legend. Features of HPV16 integration (solid box) and host rearrangement (dotted) sites are depicted as single-letter icons. DNA copy number (CN) is displayed in gradient red colour (light-blue for regions outside of the LGM), with bilateral labels

in relevant sample colour. The HPV16 genome reference is NC 001526.4 from the NCBI Nucleotide database.

Figure 6. Features of HBV integrated LGMs in six HCC samples. Human genomic segments related to HBV integrated LGMs are shown as sectors with their relevant LGM path in sample specific colours. Segments of LGMs are denoted by numbered concentric arcs. The numbers, starting from 1, indicate the order in which each arc is visited starting from the source segment of an LGM. Sequential segments in LGM could be merged in single arc (**Supplementary Table S9**). Repeat times of unit-cycles in LGMs are stated in figure legend. Features of HBV integrated sites are depicted as single-letter icons. DNA copy number (CN) is displayed in gradient red colour (light-blue for regions outside of the LGM), with bilateral labels in relevant sample colour. The HBV genome reference is FJ899779.1 from the NCBI Nucleotide database.

Supplementary Data

Supplementary Table S1. Details of simulated oncovirus integrated local genomic map.

Supplementary Table S2. Mutations used to reconstruct HPV genomes in six HPV-infected cancer samples.

Supplementary Table S3. Details of local genomic map in four cervical carcinoma samples.

Supplementary Table S4. Details of local genomic map in two HPV infected HNSCC cancer cell lines.

Supplementary Table S5. Mutations used to reconstruct HBV genomes in six HBV-infected HCC samples.

Supplementary Table S6. Details of local genomic map in six HBV infected HCC samples.

Supplementary Table S7. Local genomic map of one complex SV on chr12 of GBM0152 sample.

Supplementary Table S8. MHs and insertions at the junction sites in resolved local genomic maps.

Supplementary Table S9. Relationship of segment IDs in LGMcircos and LGM.

Supplementary Figure S1. The eight LGM modes in simulation work are denoted with features and represented by basic structures.

Supplementary Figure S2. Copy number distribution along the HPV-integrated chromosome in four cervical cancer samples [7].

Supplementary Figure S3. Presentative LGM at HPV integration sites (gene GLI2) on chr2 (major allele) of the T4931 sample [7].

Supplementary Figure S4. Presentative LGM at HPV integration sites (upstream of gene MYC) on chr8 (major allele) of the HeLa cell line [7].

Supplementary Figure S5. Presentative LGM at HPV integration sites (gene KLF12) on chr13 (LOH) of the T6050 sample [7].

Supplementary Figure S6. Presentative LGM at HPV integration sites (upstream of gene KLF12) on chr13 (LOH) of the SiHa cell line [7].

Supplementary Figure S7. Copy number distribution along the HPV-integrated chromosome in two HNSCC cell lines [2].

Supplementary Figure S8. Presentative LGM at HPV integration sites (gene TP63) on chr3 (minor allele) of the UM-SCC-47 cell line [2].

Supplementary Figure S9. Presentative LGM at HPV integration sites (gene TP63) on chr3 (major allele) of the UM-SCC-47 cell line [2].

Supplementary Figure S10. Presentative LGM at HPV integration sites (gene PIM1) on chr6 (minor allele) on chr6 of the UPCI-SCC090 cell line [2].

Supplementary Figure S11. Presentative LGM at HPV integration sites (gene PIM1) on chr6 (major allele) of the UPCI-SCC090 cell line [2].

Supplementary Figure S12. Copy number distribution along the HBV-integrated chromosome in six HCC samples [11].

Supplementary Figure S13. Presentative LGM at HBV integration sites (gene NBAS) on chr2 of the 182T HCC sample [11].

Supplementary Figure S14. Presentative LGM at HBV integration sites (gene TERT) on chr5 (minor allele) of the 13T HCC sample [11].

Supplementary Figure S15. Presentative LGM at HBV integration sites (gene ANK3) on chr10 of the 260T HCC sample [11].

Supplementary Figure S16. Presentative LGM at HBV integration sites (gene GLRA2) on chrX of the 101T HCC sample [11].

Supplementary Figure S17. Presentative LGM at HBV integration sites (gene BBS2) on chr16 of the 261T HCC sample [11].

Supplementary Figure S18. Presentative LGM at complex SV locus on chr12 of the GBM0152 cancer sample [15].

Supplementary Figure S19. Alignment of the sequence around the integration site between the human genome and the HPV16 genome, and the endogenous rearrangements on human genome and the HPV16 genome respectively, in the T4931 sample [7].

Supplementary Figure S20. Alignment of the sequence around the integration site between the human genome and the HPV16 genome, and the endogenous rearrangements on human genome, in the T6050 sample [7].

Supplementary Figure S21. Alignment of the sequence around the integration site between the human genome and the HPV16 genome, and the endogenous rearrangements on human genome and the HPV16 genome respectively, in the UM-SCC-47 cell line [2].

Supplementary Figure S22. Alignment of the sequence around the integration site between the human genome and the HPV16 genome, and the endogenous rearrangements on human genome and the HPV16 genome respectively, in the UPCI-SCC090 cell line [2].

Supplementary Figure S23. Alignment of the sequence around the integration site between the human genome and the HBV genome, and the endogenous rearrangements on HBV genome, in the 13T HCC sample [11].

Supplementary Figure S24. Alignment of the sequence around the integration site between the human genome and the HBV genome in the 182T HCC sample [11].

Supplementary Figure S25. Alignment of the sequence around the integration site between the human genome and the HBV genome, and the endogenous rearrangements on HBV genome, in the 260T HCC sample [11].

Supplementary Figure S26. Alignment of the sequence around the integration site between the human genome and the HBV genome, and the endogenous rearrangements on HBV genome, in the 261T HCC sample [11].

Supplementary Figure S27. Alignment of the sequence around the endogenous complex rearrangements on human genome in the GBM0152 cancer sample [15].

Supplementary Figure S28. Features of the complex SV LGM in GBM0152 sample. Human genomic segments related to complex SVs LGMs are shown as sectors with their relevant LGM path.

Supplementary Figure S29. Features of HPV18 integrated LGM in HeLa cell line.

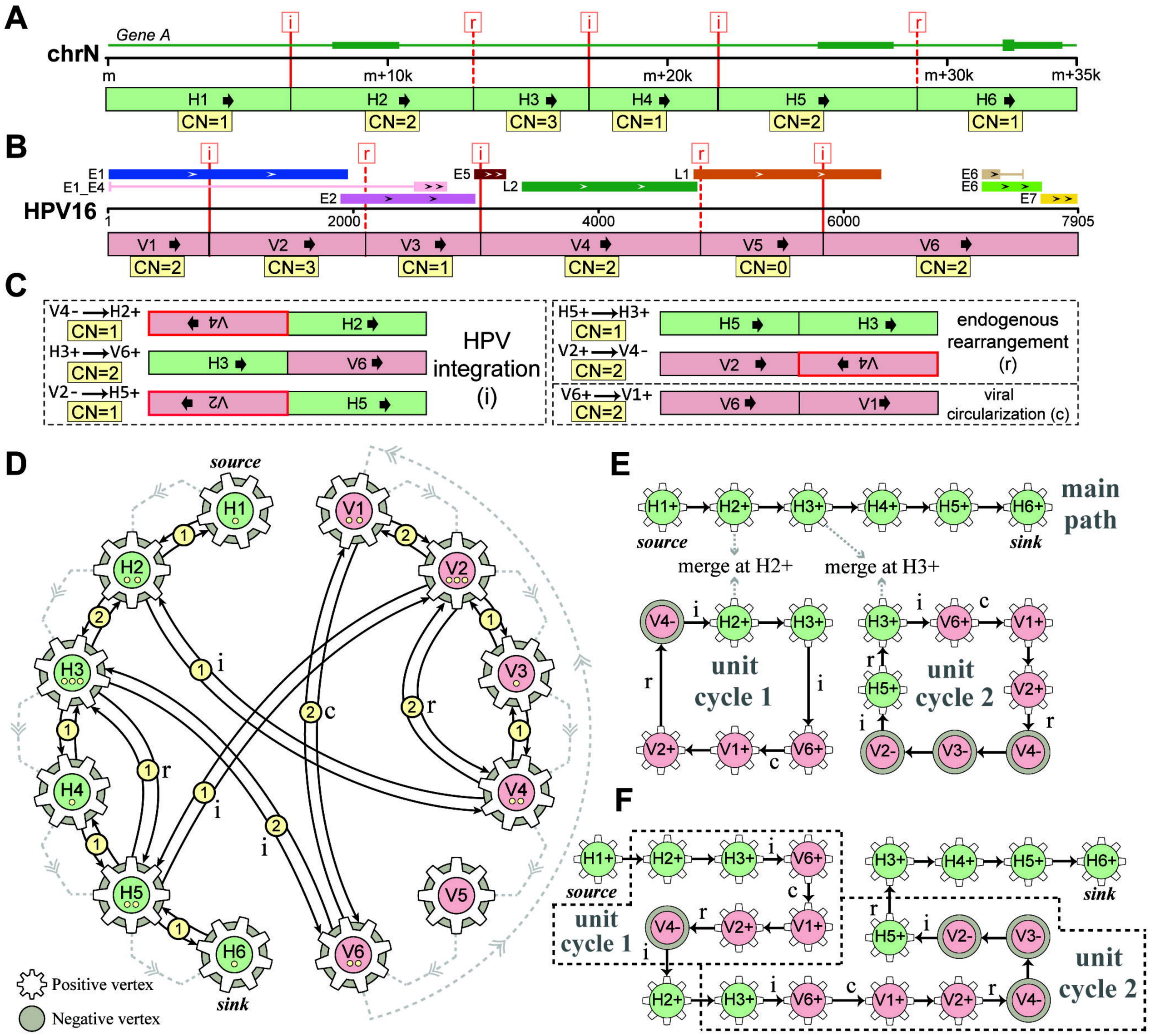
A
Gene A
chrN
m
m+10k
m+20k
m+30k
m+35k
H1
H2
H3
H4
H5
H6
CN=1
CN=2
CN=3
CN=1
CN=2
CN=1
B
HPV16
E1
E1_E4
E2
E5
L2
L1
E6
E6
E7
1
2000
4000
6000
7905
V1
V2
V3
V4
V5
V6
CN=2
CN=3
CN=1
CN=2
CN=0
CN=2
C
V4- → H2+
CN=1
H3+ → V6+
CN=2
V2- → H5+
CN=1
HPV integration (i)
H5+ → H3+
CN=1
V2+ → V4-
CN=2
endogenous rearrangement (r)
V6+ → V1+
CN=2
viral circularization (c)
D
source
sink
Positive vertex
Negative vertex
E
main path
source
sink
merge at H2+
merge at H3+
unit cycle 1
unit cycle 2
F
source
sink
unit cycle 1
unit cycle 2

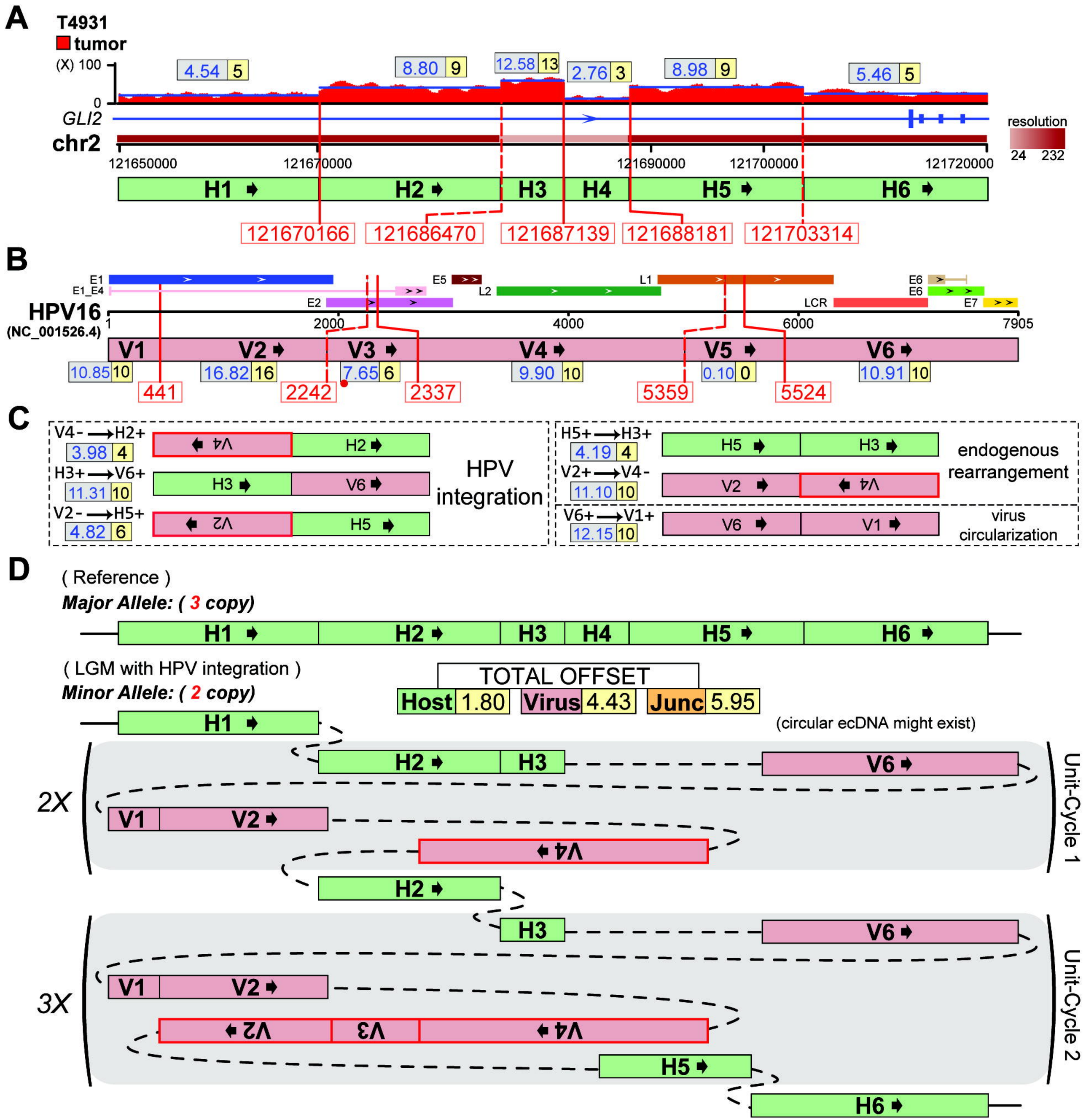
A
T4931
tumor
(X) 100
0
4.54 5
8.80 9
12.58 13
2.76 3
8.98 9
5.46 5
GLI2
chr2
resolution
24 232
121650000
121670000
121690000
121700000
121720000
H1
H2
H3
H4
H5
H6
121670166
121686470
121687139
121688181
121703314
B
E1
E1_E4
E2
E5
L2
L1
LCR
E6
E6
E7
HPV16
(NC_001526.4)
1
2000
4000
6000
7905
V1
V2
V3
V4
V5
V6
10.85 10
16.82 16
7.65 6
9.90 10
0.10 0
10.91 10
441
2242
2337
5359
5524
C
V4- → H2+
3.98 4
H3+ → V6+
11.31 10
V2- → H5+
4.82 6
HPV integration
H5+ → H3+
4.19 4
V2+ → V4-
11.10 10
endogenous rearrangement
V6+ → V1+
12.15 10
virus circularization
D
(Reference)
Major Allele: (3 copy)
(LGM with HPV integration)
Minor Allele: (2 copy)
TOTAL OFFSET
Host 1.80
Virus 4.43
Junc 5.95
(circular ecDNA might exist)
2X
3X
Unit-Cycle 1
Unit-Cycle 2

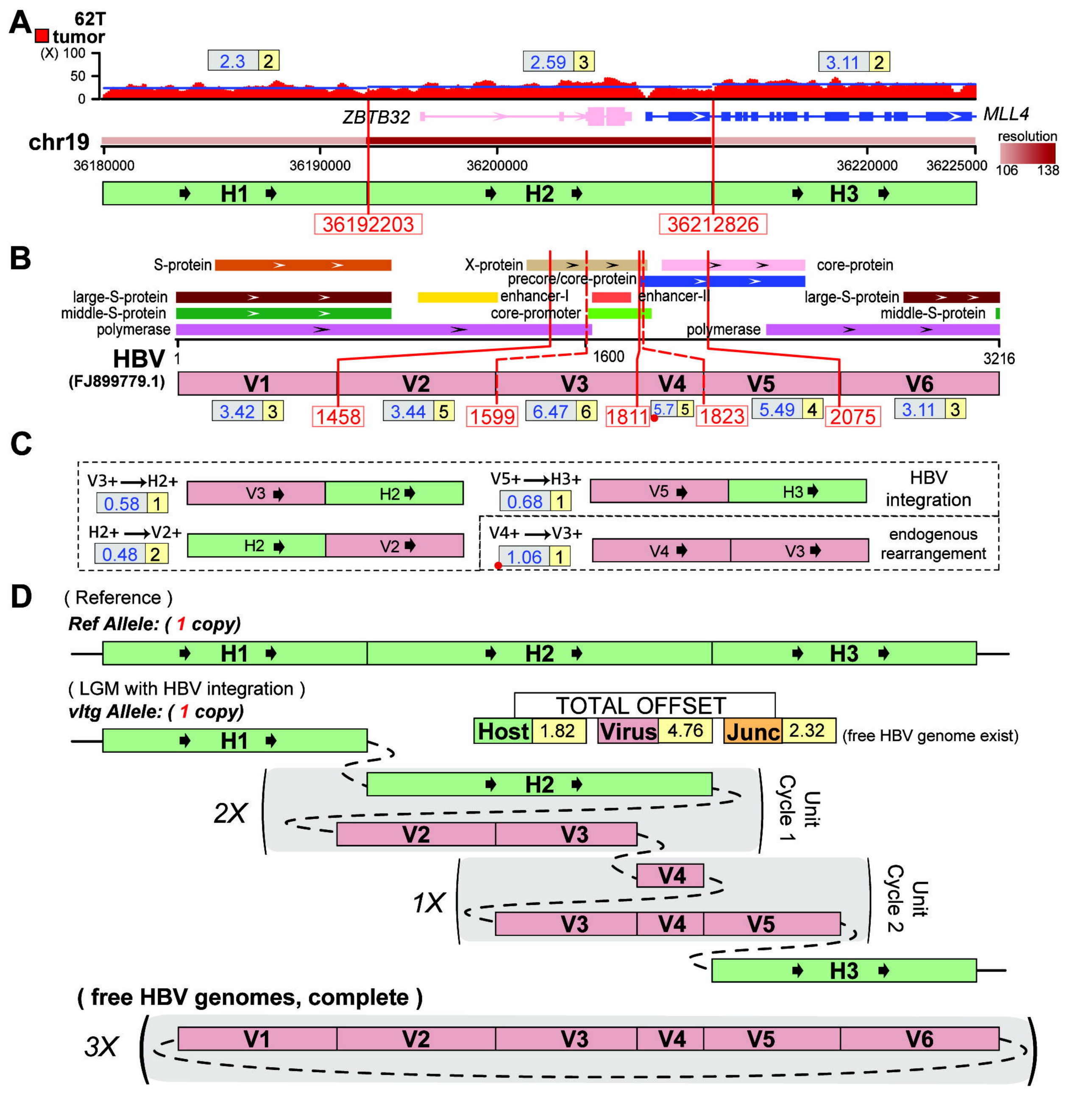
A
62T
tumor
(X) 100
50
0
2.3 2
2.59 3
3.11 2
ZBTB32
MLL4
chr19
resolution
106 138
36180000
36190000
36200000
36220000
36225000
H1
H2
H3
36192203
36212826
B
S-protein
X-protein
core-protein
precore/core-protein
large-S-protein
enhancer-I
enhancer-II
large-S-protein
middle-S-protein
core-promoter
middle-S-protein
polymerase
polymerase
HBV
(FJ899779.1)
1
1600
3216
V1
V2
V3
V4
V5
V6
3.42 3
1458
3.44 5
1599
6.47 6
1811
5.7 5
1823
5.49 4
2075
3.11 3
C
V3+ → H2+
0.58 1
V3
H2
V5+ → H3+
0.68 1
V5
H3
HBV integration
H2+ → V2+
0.48 2
H2
V2
V4+ → V3+
1.06 1
V4
V3
endogenous rearrangement
D
(Reference)
Ref Allele: (1 copy)
H1
H2
H3
(LGM with HBV integration)
vltg Allele: (1 copy)
TOTAL OFFSET
Host 1.82
Virus 4.76
Junc 2.32
(free HBV genome exist)
H1
H2
2X
V2
V3
Unit Cycle 1
V4
1X
V3
V4
V5
Unit Cycle 2
H3
(free HBV genomes, complete)
3X
V1
V2
V3
V4
V5
V6

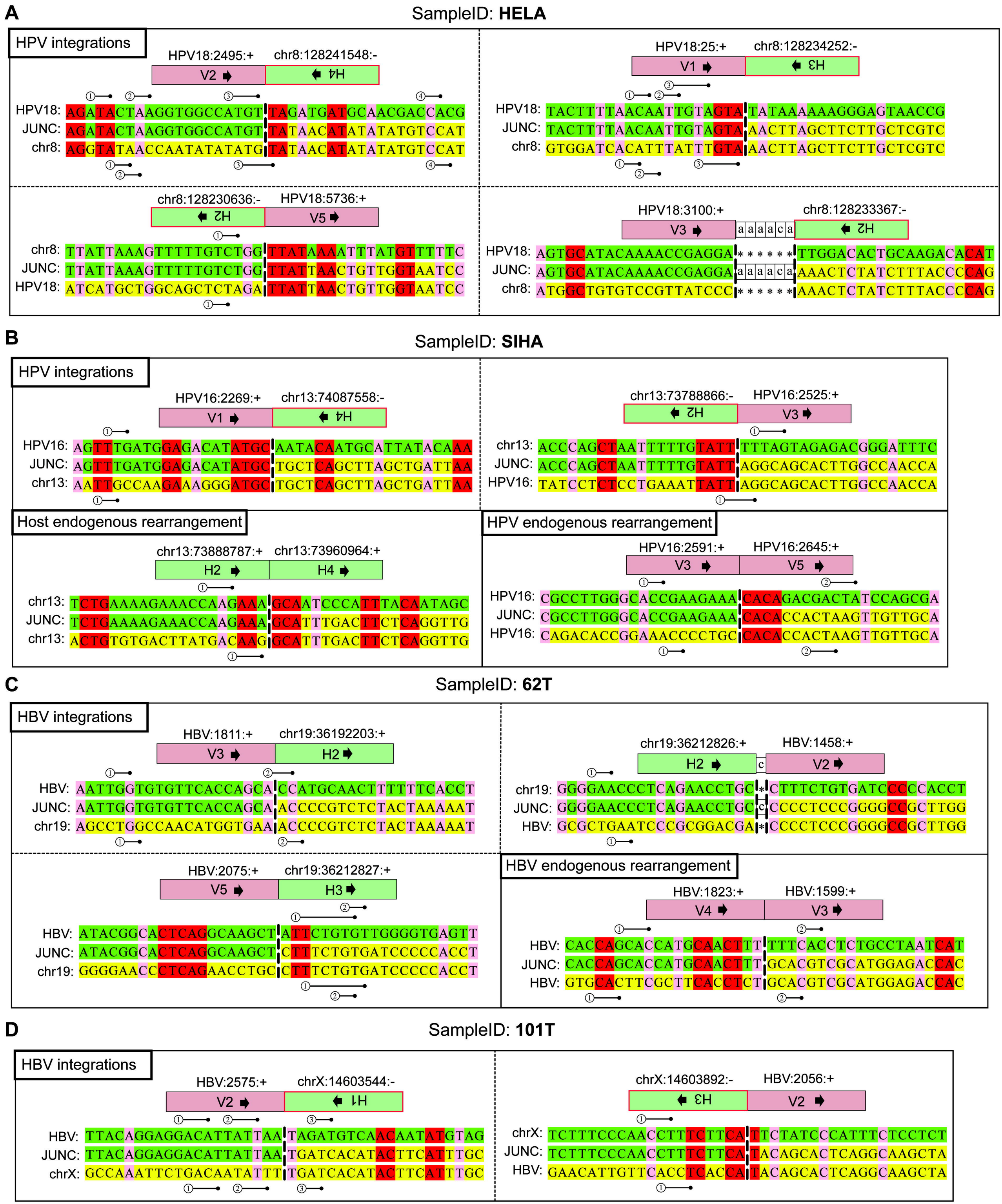
A
SampleID: HELA
HPV integrations
HPV18:2495:+
chr8:128241548:-
V2
H4
HPV18: AGATACTAAGGTGGCCATGT TAGATGATGCAACGACCACG
JUNC: AGATACTAAGGTGGCCATGT TATAACATATATATGTCCAT
chr8: AGGTATAACCAATATATATG TATAACATATATATGTCCAT
HPV18:25:+
chr8:128234252:-
V1
H3
HPV18: TACTTTTAACAATTGTAGTA TATAAAAAAGGGAGTAACCG
JUNC: TACTTTTAACAATTGTAGTA AACTTAGCTTCTTGCTCGTC
chr8: GTGGATCACATTTATTTGTA AACTTAGCTTCTTGCTCGTC
chr8:128230636:-
HPV18:5736:+
H2
V5
chr8: TTATTAAAGTTTTTGTCTGG TTATAAAATTTATGTTTTTC
JUNC: TTATTAAAGTTTTTGTCTGG TTATTAACTGTTGGTAATCC
HPV18: ATCATGCTGGCAGCTCTAGA TTATTAACTGTTGGTAATCC
HPV18:3100:+
chr8:128233367:-
V3
aaaaaca
H2
HPV18: AGTGCATACAAAACCGAGGA * * * * * * TTGGACACTGCAAGACACAT
JUNC: AGTGCATACAAAACCGAGGA aaaaaca AAACTCTATCTTTACCCCAG
chr8: ATGGCTGTGTCCGTTATCCC * * * * * * AAACTCTATCTTTACCCCAG
B
SampleID: SIHA
HPV integrations
HPV16:2269:+
chr13:74087558:-
V1
H4
HPV16: AGTTTGATGGAGACATATGC AATACAATGCATTATACAAA
JUNC: AGTTTGATGGAGACATATGC TGCTCAGCTTAGCTGATTAA
chr13: AATTGCCAAGAAAGGGATGC TGCTCAGCTTAGCTGATTAA
chr13:73788866:-
HPV16:2525:+
H2
V3
chr13: ACCCAGCTAATTTTTGTATT TTTAGTAGAGACGGGATTTC
JUNC: ACCCAGCTAATTTTTGTATT AGGCAGCACTTGGCCAACCA
HPV16: TATCCTCTCCTGAAATTATT AGGCAGCACTTGGCCAACCA
Host endogenous rearrangement
chr13:73888787:+
chr13:73960964:+
H2
H4
chr13: TCTGAAAAGAAACCAAGAAA GCAATCCCATTTACAATAGC
JUNC: TCTGAAAAGAAACCAAGAAA GCATTTGACTTCTCAGGTTG
chr13: ACTGTGTGACTTATGACAAG GCATTTGACTTCTCAGGTTG
HPV endogenous rearrangement
HPV16:2591:+
HPV16:2645:+
V3
V5
HPV16: CGCCTTGGGCACCGAAGAAA CACAGACGACTATCCAGCGA
JUNC: CGCCTTGGGCACCGAAGAAA CACACCACTAAGTTGTTGCA
HPV16: CAGACACCGGAAACCCCTGC CACACCACTAAGTTGTTGCA
C
SampleID: 62T
HBV integrations
HBV:1811:+
chr19:36192203:+
V3
H2
HBV: AATTGGTGTGTTCACCAGCA CCATGCAACTTTTTCACCT
JUNC: AATTGGTGTGTTCACCAGCA ACCCCGTCTCTACTAAAAAT
chr19: AGCCTGGCCAACATGGTGAA ACCCCGTCTCTACTAAAAAT
chr19:36212826:+
HBV:1458:+
H2
c
V2
chr19: GGGGAACCCTCAGAACCTGC * CTTTCTGTGATCCCCCACCT
JUNC: GGGGAACCCTCAGAACCTGC c CCCCTCCCGGGGCCGCTTGG
HBV: GCGCTGAATCCCGCGGACGA * CCCCTCCCGGGGCCGCTTGG
HBV:2075:+
chr19:36212827:+
V5
H3
HBV: ATACGGCACTCAGGCAAGCT ATTCTGTGTTGGGGTGAGTT
JUNC: ATACGGCACTCAGGCAAGCT CTTTCTGTGATCCCCCACCT
chr19: GGGGAACCCTCAGAACCTGC CTTTCTGTGATCCCCCACCT
HBV endogenous rearrangement
HBV:1823:+
HBV:1599:+
V4
V3
HBV: CACCAGCACCATGCAACTTT TTTCACCTCTGCCTAATCAT
JUNC: CACCAGCACCATGCAACTTT GCACGTCGCATGGAGACCAC
HBV: GTGCACTTCGCTTCACCTCT GCACGTCGCATGGAGACCAC
D
SampleID: 101T
HBV integrations
HBV:2575:+
chrX:14603544:-
V2
H1
HBV: TTACAGGAGGACATTATTAA TAGATGTCAACAATATGTAG
JUNC: TTACAGGAGGACATTATTAA TGATCACATACTTCATTTGC
chrX: GCCAAATTCTGACAATATTT TGATCACATACTTCATTTGC
chrX:14603892:-
HBV:2056:+
H3
V2
chrX: TCTTTCCCAACCTTTCTTCA TTCTATCCCATTTCTCCTCT
JUNC: TCTTTCCCAACCTTTCTTCA TACAGCACTCAGGCAAGCTA
HBV: GAACATTGTTCACCTCACCA TACAGCACTCAGGCAAGCTA

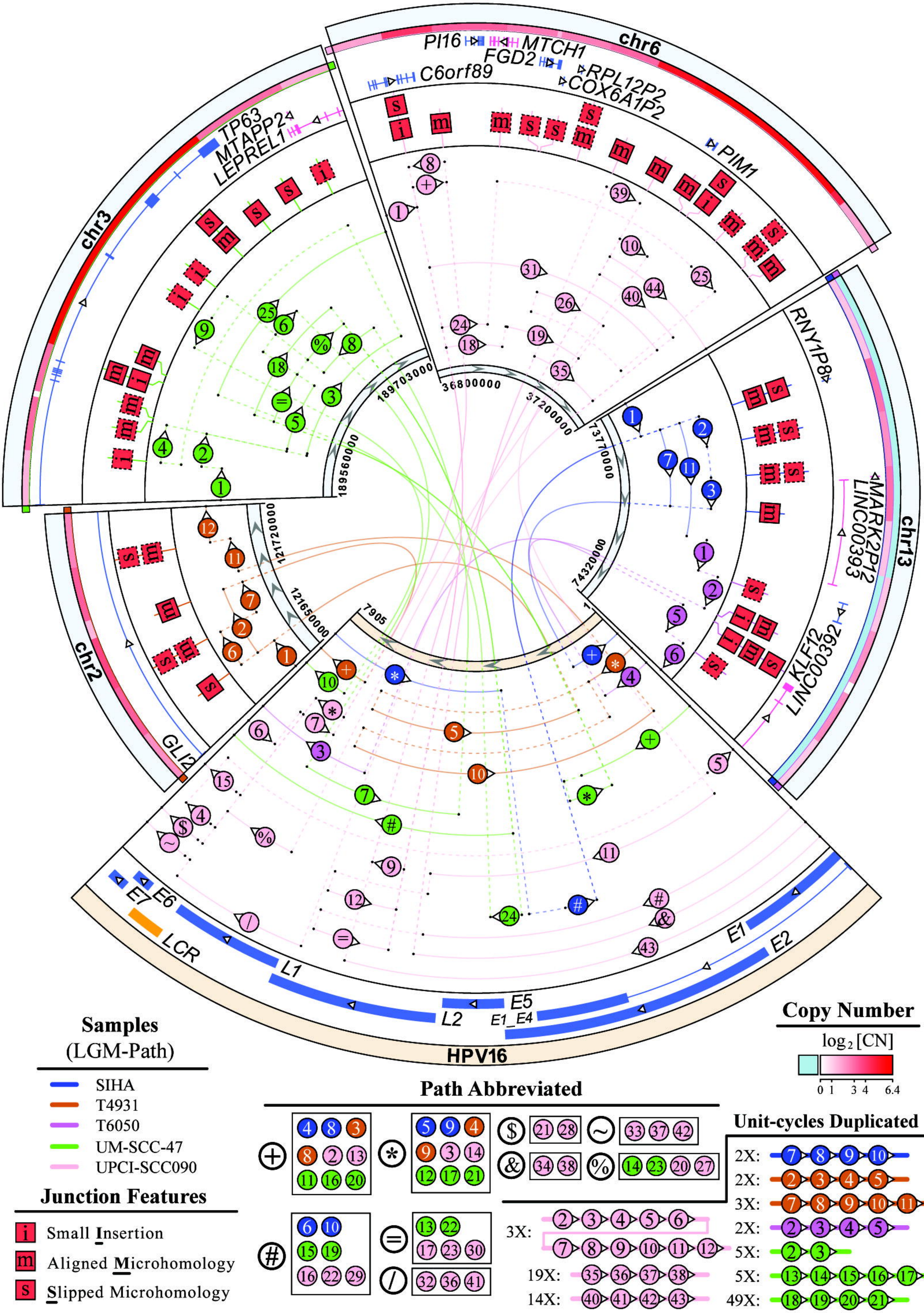
chr6
PI16
MTCH1
FGD2
C6orf89
RPL12P2
COX6A1P2
PIM1
chr3
TP63
MTAPP2
LEPREL1
chr13
RNY1P8
MARK2P12
LINC00393
KLF12
LINC00392
chr2
GLI2
189703000
36800000
37200000
73770000
74320000
189560000
121720000
121650000
7905
1
HPV16
E7
E6
LCR
L1
L2
E5
E1_E4
E1
E2
Samples
(LGM-Path)
SIHA
T4931
T6050
UM-SCC-47
UPCI-SCC090
Junction Features
i Small Insertion
m Aligned Microhomology
s Slipped Microhomology
Path Abbreviated
Copy Number
log2 [CN]
0 1 3 4 6.4
Unit-cycles Duplicated
2X:
2X:
3X:
2X:
5X:
5X:
49X:
3X:
19X:
14X:

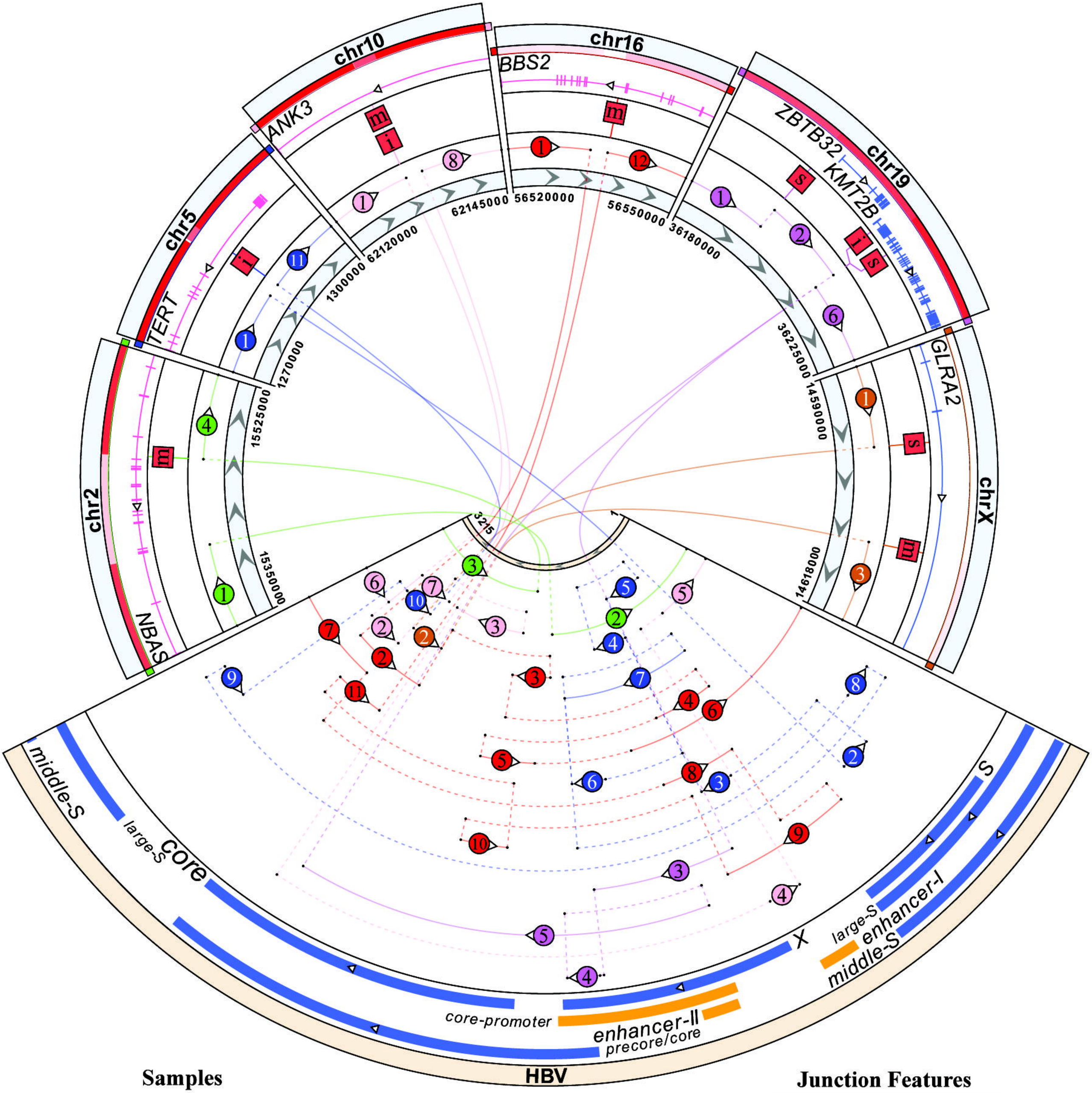
chr10
chr16
chr19
chr5
chr2
chrX
ANK3
BBS2
ZBTB32
KMT2B
TERT
GLRA2
NBAS
62145000
56520000
56550000
36180000
62120000
1300000
1270000
1552500
1535000
3215
36225000
1459000
1461800
HBV
core
middle-S
large-S
S
X
core-promoter
enhancer-II
precore/core
enhancer-I
Samples
(LGM-Path)
13T
62T
101T
182T
260T
261T
Unit-cycles Duplicated
2X:
2X:
Copy Number
log2 [CN]
0
1
2
Junction Features
Small Insertion
Aligned Microhomology
Slipped Microhomology